ULF wave derived radiation belt radial diffusion coefficients

Louis G. Ozeke,[1] Ian R. Mann,[1] Kyle R. Murphy,[1] I. Jonathan Rae,[1] David K. Milling,[1] Scot R. Elkington,[2] Anthony A. Chan,[3] and Howard J. Singer[4]

Received 16 December 2011; revised 14 February 2012; accepted 23 February 2012; published 24 April 2012.

[1] Waves in the ultra-low-frequency (ULF) band have frequencies which can be drift resonant with electrons in the outer radiation belt, suggesting the potential for strong interactions and enhanced radial diffusion. Previous radial diffusion coefficient models such as those presented by Brautigam and Albert (2000) have typically used semiempirical representations for both the ULF wave's electric and magnetic field power spectral densities (PSD) in space in the magnetic equatorial plane. In contrast, here we use ground- and space-based observations of ULF wave power to characterize the electric and magnetic diffusion coefficients. Expressions for the electric field power spectral densities are derived from ground-based magnetometer measurements of the magnetic field PSD, and in situ AMPTE and GOES spacecraft measurements are used to derive expressions for the compressional magnetic field PSD as functions of Kp, solar wind speed, and L-shell. Magnetic PSD results measured on the ground are mapped along the field line to give the electric field PSD in the equatorial plane assuming a guided Alfvén wave solution and a thin sheet ionosphere. The ULF wave PSDs are then used to derive a set of new ULF-wave driven diffusion coefficients. These new diffusion coefficients are compared to estimates of the electric and magnetic field diffusion coefficients made by Brautigam and Albert (2000) and Brautigam et al. (2005). Significantly, our results, derived explicitly from ULF wave observations, indicate that electric field diffusion is much more important than magnetic field diffusion in the transport and energization of the radiation belt electrons.

Citation: Ozeke, L. G., I. R. Mann, K. R. Murphy, I. J. Rae, D. K. Milling, S. R. Elkington, A. A. Chan, and H. J. Singer (2012), ULF wave derived radiation belt radial diffusion coefficients, *J. Geophys. Res.*, *117*, A04222, doi:10.1029/2011JA017463.

1. Introduction

[2] The Earth's outer radiation belt was unexpectedly discovered by Explorer 1 observations at the beginning of the space age [*Van Allen et al.*, 1958]. However, after over 50 years of in situ measurements there is no universally accepted dominant mechanism responsible for the energization and dynamics of relativistic electrons trapped in the Earth's geomagnetic field. *Fälthammar* [1965] proposed that fluctuations in the geomagnetic field produced by ultra-low-frequency (ULF) waves may cause adiabatic radial diffusion of the radiation belt electrons. In this model, electrons gain energy as they are radially transported inward from the plasma sheet to the radiation belts under the action of fluctuating electric and magnetic fields conserving their first adiabatic invariant. However, in order to determine the importance of radial diffusion for outer radiation belt electron dynamics, the power spectral density (PSD) of the ULF wave's azimuthal electric and compressional magnetic field fluctuations in space in the magnetic equatorial plane must be determined. Several different previous approaches have been used to determine these ULF wave electric and magnetic field power spectral densities.

[3] *Holzworth and Mozer* [1979] characterized the electric field diffusion term by using balloon measurements of ULF wave electric field PSDs at $L = 6$ in the ionosphere and, by assuming that the field lines were electric equipotentials, mapped these ionospheric electric fields to the magnetic equatorial plane to obtain an equatorial electric field PSD in space. Using these electric field PSD estimates, the electric field diffusion coefficient was derived at $L = 6$ [*Holzworth and Mozer*, 1979]. *Cornwall* [1968] derived an analytic expression for the electric field diffusion coefficient by assuming that the electric field spectrum can be modeled as a substorm convection electric field characterized by a rapid risetime and an exponential decay. A similar approach was used by *Brautigam and Albert* [2000] to estimate the electric field diffusion coefficients. More recently in situ CRRES measurements made from January to October 1991 of the electric field PSD close to the magnetic equatorial plane

[1]Department of Physics, University of Alberta, Edmonton, Alberta, Canada.
[2]Laboratory for Atmospheric and Space Physics, University of Colorado at Boulder, Boulder, Colorado, USA.
[3]Department of Physics and Astronomy, Rice University, Houston, Texas, USA.
[4]Space Weather Prediction Center, NOAA, Boulder, Colorado, USA.

0148-0227/12/2011JA017463

have been used to derive the electric field diffusion coefficient as a function of Kp and L-shell [*Brautigam et al.*, 2005].

[4] For magnetic diffusion, *Brautigam and Albert* [2000] derived an analytic expression for the compressional magnetic field diffusion coefficient as a function of Kp and L-shell based on measurements of the magnetic field PSD at $L = 4$ on the ground and at $L = 6.6$ in space. The ground magnetic field PSD measurements were mapped to the equatorial plane using the technique discussed by *Lanzerotti and Morgan* [1973], which assumes azimuthally symmetric compressional magnetic field fluctuations in a dipole model of the Earth's magnetic field. *Brautigam et al.* [2005] showed that the magnetic field diffusion coefficients derived by *Brautigam and Albert* [2000] using the mapping assumption of *Lanzerotti and Morgan* [1973] are dominant over the electric field diffusion coefficients estimated both from CRRES electric field PSD measurements [*Brautigam et al.*, 2005] and from the convection electric field model [*Cornwall*, 1968; *Brautigam and Albert*, 2000].

[5] In this paper we determine electric field diffusion coefficients based on over 15 years of ground magnetometer measurements of the magnetic field PSD mapped to the electric field PSD in the equatorial plane using the guided Alfvén wave mapping model discussed by *Ozeke et al.* [2009] and *Rae et al.* [2012]. In situ measurements of the compressional magnetic field PSD made using the AMPTE and GOES spacecraft are also used to derive expressions for the magnetic field diffusion coefficients.

2. Radial Diffusion Coefficients

[6] The radial diffusion equation expressed in terms of L-shell is given by

$$\frac{\partial f}{\partial t} = L^2 \frac{\partial}{\partial L}\left[\frac{D_{LL}}{L^2}\frac{\partial f}{\partial L}\right] \tag{1}$$

In equation (1) f represents the phase space density of the electrons, and it is assumed that the first and second adiabatic invariants, M and J, are conserved [see *Schulz and Lanzerotti*, 1974].

[7] The diffusion coefficient, D_{LL}, is the sum of the diffusion coefficients due to the electric and compressional magnetic field perturbations D_{LL}^E and D_{LL}^B. In a dipole magnetic field, the diffusion coefficients due to the electric and magnetic field perturbations D_{LL}^E and D_{LL}^B can be expressed as

$$D_{LL}^E = \frac{1}{8B_E^2R_E^2}L^6\sum_m P_m^E(m\omega_d) \tag{2}$$

$$D_{LL}^E = \frac{M^2}{8q^2\gamma^2B_E^2R_E^4}L^4\sum_m m^2P_m^B(m\omega_d) \tag{3}$$

$$M = \frac{p_\perp^2 L^3}{2m_eB_E} \tag{4}$$

[see *Fälthammar*, 1965; *Brizard and Chan*, 2001; *Fei et al.*, 2006]. Here the constants B_E, R_E, and q represent the equatorial magnetic field strength at the surface of the Earth, the Earth's radius, and the electron charge, respectively. The relativistic correction factor, γ, given by

$$\gamma = \left(1 - v^2/c^2\right)^{-1/2}, \tag{5}$$

where v is the total speed of the electron and c is the speed of light, does not remain constant but increases and decreases as the electrons diffuse radially inward and outward, respectively. M represents the first adiabatic invariant which depends on the electrons mass m_e and the perpendicular momentum $p_\perp$ (see equation (4)).

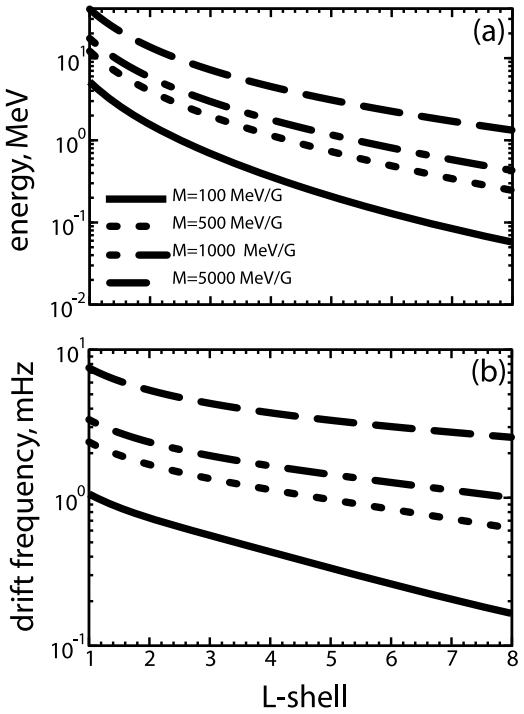

Figure 1. (a) Electron resonant energies and (b) Electron drift frequencies, which satisfy the $m = 1$ drift resonance conditions with M-values 100, 500, 1000 and 5000 MeV/G.

[8] In equations (2) and (3) the terms $P_m^E(m\omega_d)$ and $P_m^B(m\omega_d)$ represent the PSD of the electric and magnetic field perturbations with azimuthal wave number m at wave frequencies ω which satisfy the drift resonance condition given by

$$\omega - m\omega_d = 0. \tag{6}$$

Here, ω_d represents the bounce-averaged angular drift frequency of the electron [see *Southwood and Kivelson*, 1982; *Brizard and Chan*, 2001]. Since ω_d is a function of the electron's energy and L-shell, this introduces an energy and L-shell dependence into the PSD terms $P_m^E(m\omega_d)$ and $P_m^B(m\omega_d)$ in equations (2) and (3). Figure 1 illustrates how the electron energy and drift frequency vary as a function of L-shell for electron's with M-values of 100, 500, 1000, and 5000 MeV/G, where G is in Gauss.

[9] The electric and magnetic field diffusion coefficients shown in equations (2) and (3) can be added together to form the total diffusion coefficient D_{LL}^{Total}, where

$$D_{LL}^{Total} = D_{LL}^E + D_{LL}^B \tag{7}$$

In a dipole field, only the azimuthal electric field (which is parallel to the electron's drift velocity) produced by the shear Alfvén wave should be used in equation (2) to determine D_{LL}^{E}. Any azimuthal electric field resulting from the compressional fast mode should not be included in the calculation of D_{LL}^{E}, since the diffusive effect of this fast mode wave is already included in the calculation of D_{LL}^{B}, and should not be counted twice. Observationally it may be difficult to separate these two potential sources of electric field perturbations, especially for in situ measurements. Our approach here explicitly assumes that the D-component magnetic field measurement we use from the ground only contains Alfvénic contributions which map to the azimuthal electric field in space. By using in situ compressional magnetic field measurements, to specify D_{LL}^{B}, we aim to minimize any multiple counting arising from the coupling between wave electric and magnetic fields through Faraday's law.

2.1. Mapped Ground Magnetic Field PSD to Electric Field PSD in Space

[10] To directly measure the required electric and magnetic field PSDs and wave *m*-values would require multiple simultaneous measurements of the global structure and variability of the wave's electric and magnetic fields in space in the equatorial plane [cf. *Brautigam et al.*, 2005]. However, this would require the deployment of multisatellite constellations in the radiation belt region. Instead of using in situ measurements of electric field PSD, to determine ULF wave driven diffusion coefficients we use ground-based magnetometer measurements to obtain the magnetic PSD on the ground, and map these magnetic field PSDs to the electric field PSD in space in the equatorial plane using the Alfvénic wave mapping model described by *Ozeke et al.* [2009] and the results within *Rae et al.* [2012].

[11] In this study we use the same database of hourly PSD estimates taken using the CARISMA [*Mann et al.*, 2008] and SAMNET [*Yeoman et al.*, 1990] magnetometer stations over a period of approximately 15 years discussed by *Rae et al.* [2012, section 2]. However, here we determine the median D-component PSDs binned with Kp and solar wind speed using the hourly PSD estimates derived for windows 1 h in length taken only from the dayside between 0600 LT and 1800 LT.

[12] The Alfvénic mapping model used to determine the equatorial electric field PSD from the PSD measured on the ground assumes a dipole magnetic field. Since this dipole approximation is a poor representation of the Earth's magnetic field on the nightside of the magnetosphere, especially at high L-shells, we choose to characterize D_{LL}^{E} using only PSD measured on the dayside from approximately 0600 to 1800 MLT. Moreover, in order to represent the power in the azimuthal electric field in space we average the D-component ground-based magnetic field component, which is expected to represent a poloidally polarized mode with an azimuthal electric field after an Alfvénic polarization rotation of 90° through the ionosphere [cf. *Hughes and Southwood*, 1976; *Kivelson and Southwood* 1988]. Median D-component magnetic PSD values, averaged over 12 h of MLT from 0600 to 1800 MLT, are illustrated in Figure 2 for the bins with Kp-values of 1, 3 and 6. Figure 2 shows that in general the log of the magnetic field PSD on the ground varies approximately linearly with the log of the frequency, with a slight change in the gradient of the slope occurring at ~4 mHz.

[13] In the work by *Brautigam et al.* [2005] the in situ CRRES measurements of the electric field PSD in the equatorial plane were binned with Kp. In addition, previous models for the magnetic and electric field diffusion coefficients have also been expressed in terms of Kp [see, e.g., *Brautigam and Albert*, 2000]. In this study, the hourly median PSD values are also binned with Kp for comparison with the PSD and diffusion coefficient results presented in these previous studies. In addition, we also present electric field PSD estimates in the equatorial plane as a function of solar wind speed again obtained from the OMNI database. These estimates of the electric field PSD as a function of the solar wind speed are required for forecast and nowcast models of the radiation belt dynamics driven by the available near real time solar wind data taken from close to the L1 Lagrangian point.

[14] These D-component ground magnetic field PSDs have been mapped into space using the Alfvénic wave solution in a dipole field [see *Ozeke et al.*, 2009; *Rae et al.*, 2012] to give estimates of the equatorial azimuthal electric field PSD in space needed to determine the electric field diffusion coefficients. This mapping assumes that the equatorial azimuthal electric field results entirely from a guided Alfvén wave, with no contribution to the azimuthal electric field resulting from a compressional fast mode. This assumption is consistent with the approach discussed above used to derive equation (7), where D_{LL}^{E} is assumed to only result from the guided Alfvén wave azimuthal electric field PSD and D_{LL}^{B} is assumed to result only from the compressional magnetic field PSD.

[15] Central to this approximation is the implicit assumption that low-m standing guided Alfvén waves in the magnetosphere can have mixed polarization with electric fields which are polarized both nominally parallel (i.e., poloidal mode) and perpendicular (i.e., toroidal mode) to the direction of electron drift [see, e.g., *Cross* 1988a, 1988b]. Since in a dipole magnetic field and indeed also in more complex magnetic geometries the eigenmodes and eigenfrequencies of decoupled guided standing toroidal ($m = 0$) and guided poloidal ($m \to \infty$) modes are different, for finite values of *m* there is a natural coupling between the polarizations as the waves oscillate. Any disturbance can be constructed from a sum over these eigenmodes in each polarization, but an Alfvénic disturbance will be one which maintains a low or vanishing compressional magnetic field. In the case of undriven high but finite *m* waves, such mixed polarized modes also phase mix, which leads not only to a mixed polarization guided mode but also to an asymptotic polarization rotation from a guided poloidal to a toroidal mode in time [*Mann et al.*, 1997].

[16] As discussed by *Mann et al.* [1997], one can analyze the nature of this cross-field wave structure and polarization from the point of view of maintaining a predominantly incompressible Alfvén mode in a complex field geometry. Since the perturbed magnetic fields $\boldsymbol{b}$ must satisfy the solenoidal constraint $\nabla.\boldsymbol{b} = 0$, an Alfvénic mode with no compressional magnetic field must have $(\nabla.\boldsymbol{b})_{\perp} = 0$, which couples the two perpendicular magnetic field magnitudes in terms of the

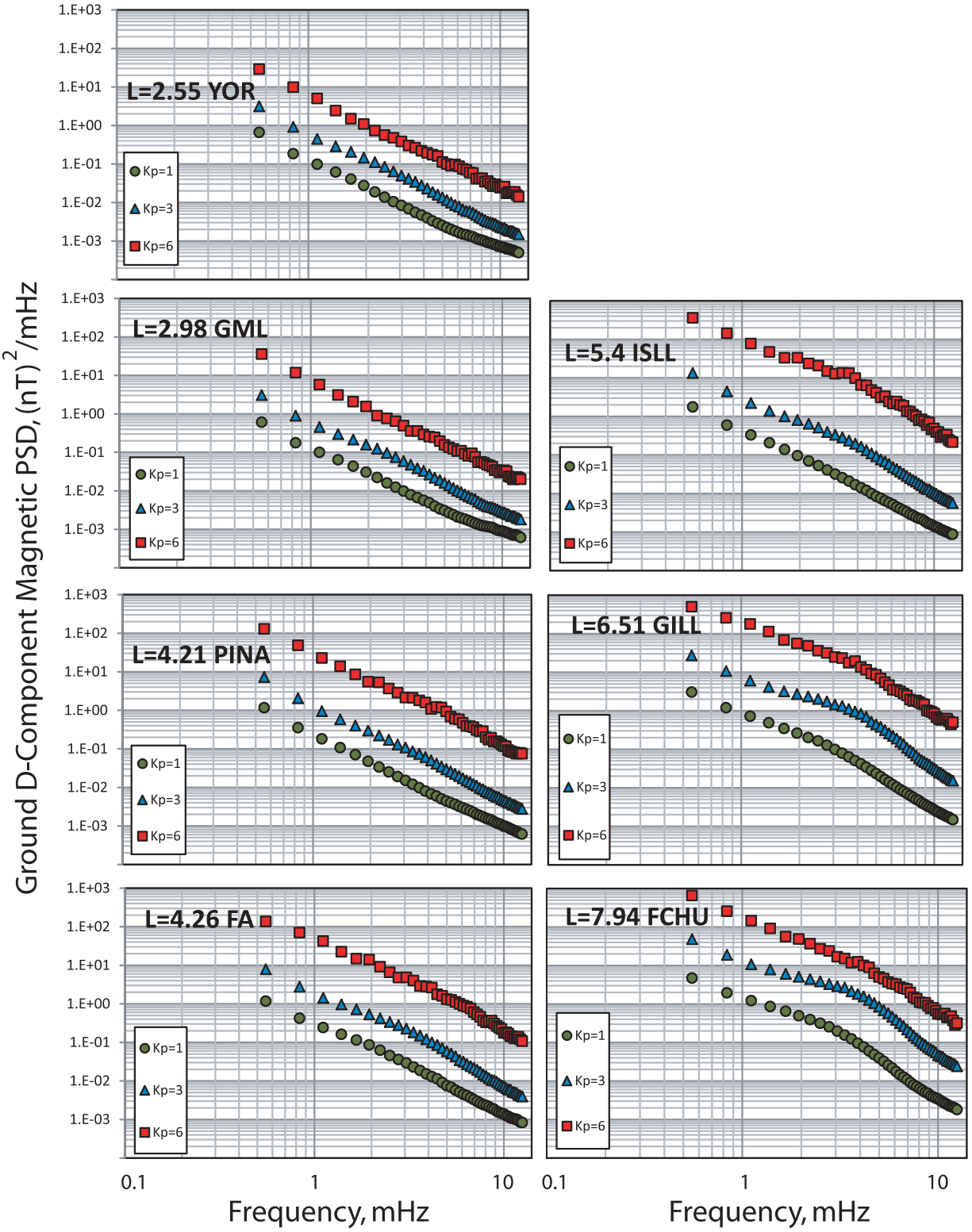

Figure 2. Median magnetic field D-component power spectral densities measured on the dayside, averaged between 0600 and 1800 MLT, and binned with Kp, using Kp-values of 1, 3 and 6.

local wave numbers. In a local Cartesian geometry with background magnetic field along $\hat{z}$, this implies

$$\frac{\partial b_x}{\partial x} + \frac{\partial b_y}{\partial y} = i\left(k_x b_x + k_y b_y\right) \approx 0, \tag{8}$$

such that the cross field scales defined by k_x and k_y determine the relative magnitudes of the perpendicular poloidal b_x and toroidal b_y mode magnetic field components. Within this paradigm, low-m Alfvénic modes can be excited with mixed polarization such that the ground-based D-component can be

mapped into an azimuthal electric field in the magnetosphere after a 90° polarization rotation upon transmission through the ionosphere. Such an approach is also validated by observations of mixed mode standing Alfvén waves in the magnetosphere. For example, *Clemmons et al.* [2000] reported a low-m ($m \sim 3$ mixed polarization mode with approximately equal poloidal and toroidal mode electric field amplitudes, with a coherent wave packet structure present in both components, and which *Ozeke et al.* [2005] interpreted as a field line resonance. Consequently, we approach the task of mapping the poloidal magnetic field component at the ionosphere b_v^i of a mixed polarization guided Alfvén wave to a poloidal electric field component in the equatorial E_φ^{eq} using the eigenfunction of a guided poloidal wave.

[17] For fundamental field aligned mode guided poloidal ULF Alfvén waves in a dipole magnetic field geometry, the relation between the radial magnetic field amplitude just above the assumed thin sheet ionosphere, b_{ob}^i, and the equatorial azimuthal electric field, E^{eq}, in space can be approximated as

$$E^{eq} = \frac{f_{ob}}{3mHz}\frac{E_\varphi^{eq}}{b_v^i}b_{ob}^i. \tag{9}$$

The value of E_φ^{eq}/b_v^i does not depend on the m-value or the latitudinal width of the wave $\Delta\theta$, however, E_φ^{eq}/b_v^i does vary as a function of L-shell as illustrated by *Ozeke et al.* [2009, Figure 5]. Equation (9) is derived by assuming a fundamental field-aligned mode guided Alfvén wave. In this paper, we assume that equation (9) can be applied to fundamental field aligned mode waves with frequencies f_{ob} in mHz which can differ from the local eigenfrequencies. The magnetic field just above the ionosphere b_{ob}^i can be estimated from the magnetic field on the ground using the relationship

$$b_{ob}^i \approx b_{ob}^g \exp\left(\left[m^2L + \frac{4\pi^2}{(\Delta\theta)^2}\right]^{1/2}\frac{h}{R_E}\right) \tag{10}$$

(see *Hughes and Southwood* [1976], *Glassmeier* [1984], and *Ozeke et al.* [2009] for more details). Here h and $\Delta\theta$ represent the height of the assumed thin sheet ionosphere above the ground, and the latitudinal width of the wave on the ground in radians, respectively (see *Ozeke et al.* [2009] for more details). In this paper we have assumed that $h = 150$ km, $\Delta\theta = 4°$, and that the azimuthal wave number, m, has a value of 1. For m-values <10, the choice of m-value has negligible effect on the mapping of b_{ob}^g to b_{ob}^i . However, varying the value of the assumed latitudinal width of the wave from $\Delta\theta = 4°$ to $\Delta\theta = 8°$ can affect the magnitude of the mapping from b_{ob}^g to b_{ob}^i by a factor of ~2, as illustrated in Figure 3.

[18] Combining equations (9) and (10) allows the D-component magnetic field measured on the ground to be mapped to the wave's equatorial azimuthal electric field in space. Consequently, the D-component magnetic field PSD, P_g^B, can be used to estimate the azimuthal electric field PSD, P_{eq}^E, using the relationship

$$P_{eq}^E = \left[\frac{E^{eq}}{b_{ob}^g}\right]^2 P_g^B. \tag{11}$$

Figure 4 shows the median electric field PSD, P_{eq}^E, mapped from the magnetic field D-component PSD, P_g^B, shown in Figure 2 again binned with Kp, with Kp-values of 1, 3 and 6 being shown in Figure 4. The peaks in the PSD are much more apparent in the electric field PSDs illustrated in Figure 4 than in the ground magnetic field PSDs illustrated in Figure 2. This is because the equatorial electric field PSD P_{eq}^E is proportional to the wave frequency, f squared, so that

$$P_{eq}^E(f) \propto f^2 P_g^B(f). \tag{12}$$

In effect the spectra P_{eq}^E is whitened by f^2 as compared to P_g^B. The gradient of the magnetic field PSD reduces slightly at approximately 4 mHz (see Figure 2). However, due to the frequency dependent mapping this slight reduction in the gradient of the ground magnetic field PSD $P_g^B(f)$ results in a peak in the electric field PSD $P_g^E(f)$ when mapped to the equatorial plane in space. This is clearly illustrated in Figure 4. Based on the measurements of the PSD $P_g^B(f)$ on the ground it appears that the ULF wave PSD can be accurately represented by a power law. However, the electric field PSD spectra $P_g^E(f)$ results clearly illustrate that a single power law does not accurately represented the electric field PSD in space. The dashed curves presented in Figure 4 show that the median electric field PSD can be accurately fitted to a power law plus a Gaussian curve characterized by the five parameters a_1, a_2, a_3, a_4 and a_5 as shown in equation (13), such that

$$\log_{10}\left[\frac{P_{eq}^E}{f^2}\right] = a_3 \exp\left[\frac{-z^2}{2}\right] + a_2 + a_1 x. \tag{13}$$

where $x = \log_{10} f$ and $z = (x - a_4)/a_5$. These five parameters are listed in Table S1 in the auxiliary material for each Kp-value ranging from 0 to 9.[1] In addition to Kp, the mapped electric field PSD values have also been binned with solar wind speed using the intervals 0–300, 300–400, 400–500, 500–600, 600–700 and > 700 km/s. The 5 parameter fits for each solar wind speed bin are listed in Table S2 in the auxiliary material. All of these fits for both Kp and solar wind speed have correlation coefficients with $R^2 > 0.9$.

[19] The clear peaks in the equatorial electric field PSD which are estimated from ground magnetic field PSD measurements P_g^B applying the *Ozeke et al.* [2009] mapping technique are in good agreement with the in situ equatorial electric field PSD values measured using CRRES presented by *Brautigam et al.* [2005]. The CRRES measured PSD and the mapped electric field PSD presented in Figure 4 both have peaks in the PSD at approximately 4 mHz, these peaks being more apparent on higher L-shells and for higher Kp-values (compare our Figure 4 with *Brautigam et al.* [2005, Figure 5]). The equatorial electric field PSDs obtained from the CRRES measurements and those which can be obtained from the mapped ground magnetic field PSD presented here are also compared in detail by *Rae et al.* [2012].

2.2. Magnetic Field PSD in Space

[20] The equatorial azimuthal electric field PSD is used to derive the electric field diffusion coefficient (see equation (2)).

[1] Auxiliary material is available in the HMTL. doi:10.1029/2011JA017463.

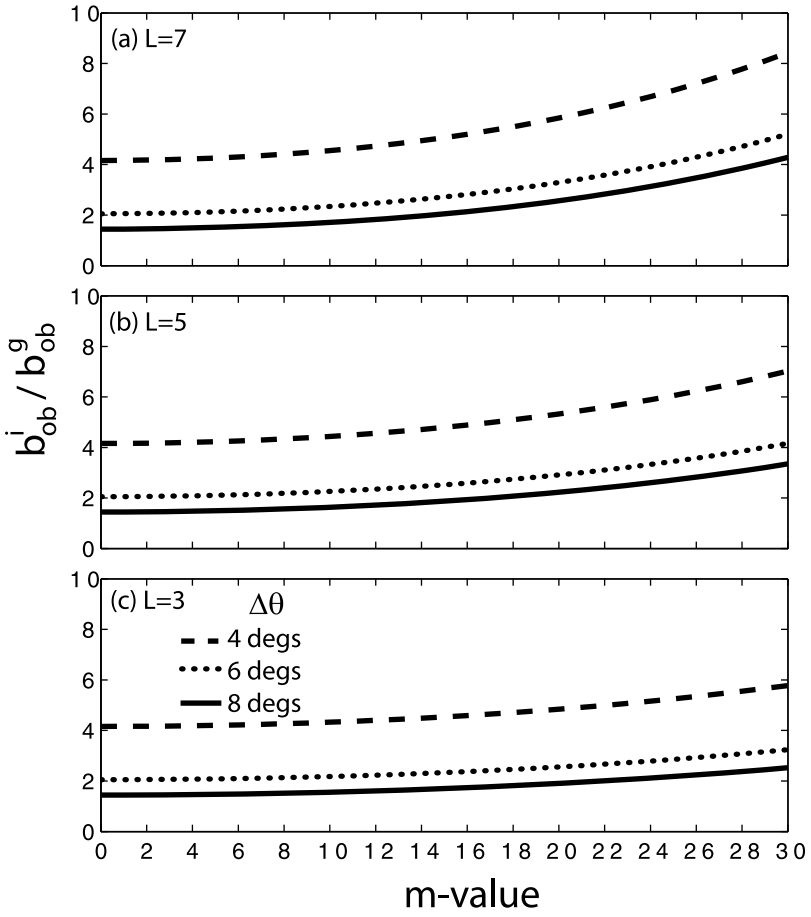

Figure 3. The dependence of the mapping scale factor on the wave's *m*-value and latitudinal width $\Delta\theta$ at L-shells of (a) $L = 7$, (b) $L = 5$ and (c) $L = 3$.

However, in order to derive the magnetic field diffusion coefficient the compressional magnetic field PSD in the equatorial plane also needs to be calculated. As presented in section 2.1 above, ground-based measurements of the D-component magnetic field can be used to estimate the equatorial electric field under an assumed Alfvénic mapping from the ground to space. Since the compressional fast wavefields in the magnetosphere in general depend on all the wave numbers in their dispersion relations, it is difficult to estimate in situ equatorial compressional fields using ground data. Indeed, mapping approaches such as *Lanzerotti and Morgan* [1973] produce results which are not a good representation of the in situ data. Instead we use empirical statistical characterizations of compressional PSD based on in situ PSD measured in space.

[21] The required compressional magnetic field PSDs in the equatorial plane at $L = 6.7$ are calculated here each hour using GOES East and West data from 1996 to 2005. The GOES magnetic field measurements have been rotated into a field-aligned coordinate system using the same method of *Rae et al.* [2005], applying a 30 min running mean. Similar to the ground magnetic field PSD analysis, the median in situ compressional wave PSDs are determined and binned with Kp and solar wind speed. However, the in situ PSD values used as input for driving D^B_{LL} are determined by averaging over 24 h MLT, as opposed to the ground magnetic magnetometer PSD values for D^E_{LL} which are averaged over the dayside from 0600 LT to 1800 LT. These median compressional magnetic field PSDs determined using the GOES data are illustrated in Figure 5 and Figure 6. Unlike the electric field PSDs the compressional magnetic field PSD in the equatorial plane can be accurately approximated by a power law as illustrated by the solid lines in Figure 5c and Figure 6c, with a correlation coefficient $R^2 > 0.9$. The functional form of the power law fits and the correlation coefficients R^2 are shown in Table 1 and Table 2 for each Kp-value or solar wind speed bin.

[22] The compressional magnetic field PSD has also been determined by *Huang et al.* [2010], using GOES data averaged over 24 MLT and binned with Kp and solar wind speed [see *Huang et al.*, 2010, Figure 6]. The PSD results presented by *Huang et al.* [2010] and in our Figures 5 and 6 are in good agreement, differing by less than a factor of 1.6. This slight difference between the *Huang et al.* [2010] PSD results and our results may result from differences in the window length and time interval. The PSDs shown by *Huang et al.* [2010, Figure 6] are determined using a window length of 3 h and GOES data from 1996 to 2003, instead of the 1 h window length and data from 1996 to 2005 used to determine our GOES PSD results presented in Figure 5 and Figure 6. Note that the *y* axis of *Huang et al.* [2010, Figure 6] is mislabeled as nT^2/mHz, the correct label being nT^2/Hz (C. L. Huang, personal communication, 2011).

[23] In both the analysis of the ground and in situ spacecraft magnetic field data, the spectral PSD values have been determined from the time series by using the method outlined

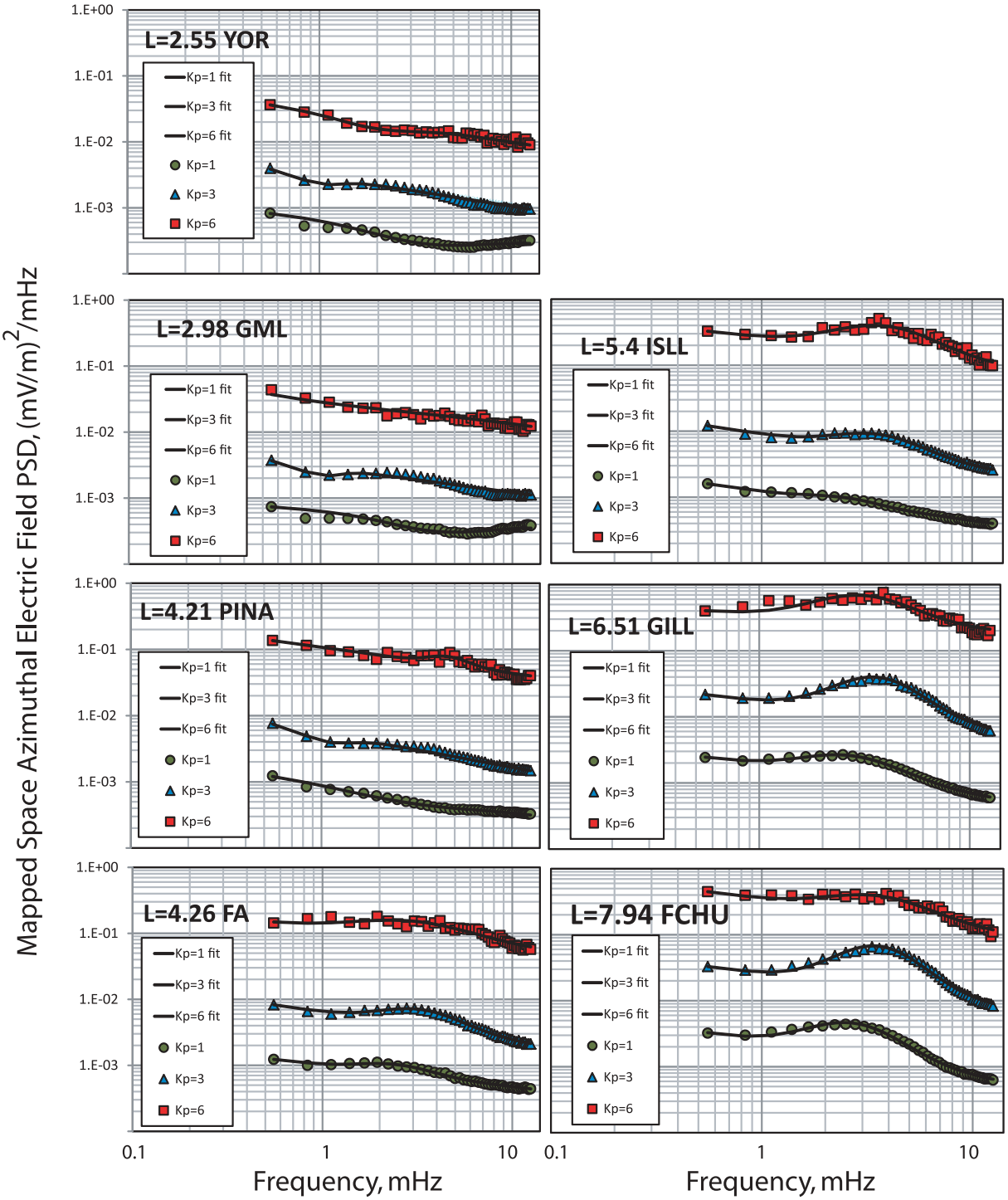

Figure 4. Azimuthal electric field power spectral densities in space in the equatorial plane obtained from the ground magnetic D-component illustrated in Figure 1. The curves illustrate the five parameter fits to these electric field power spectral density (PSD) values using the power law plus Gaussian functional form represented in equation (13).

by *Brautigam et al.* [2005] and *Rae et al.* [2012] using 1 h windows. Similar to the CRRES electric field results presented by *Brautigam et al.* [2005], our ground and in situ measured PSD values show only a slight variation with window length. Figure 7 illustrates the impact of varying the window length used for determining the PSD from the GOES East data. For Kp < 6 the PSD values are the same within a factor of about 2 for each window length shown. During high Kp intervals the magnetopause can move inward below geosynchronous altitudes so that the GOES satellites are measuring the PSD in the solar wind and not inside the magnetosphere as required. To remove these time intervals

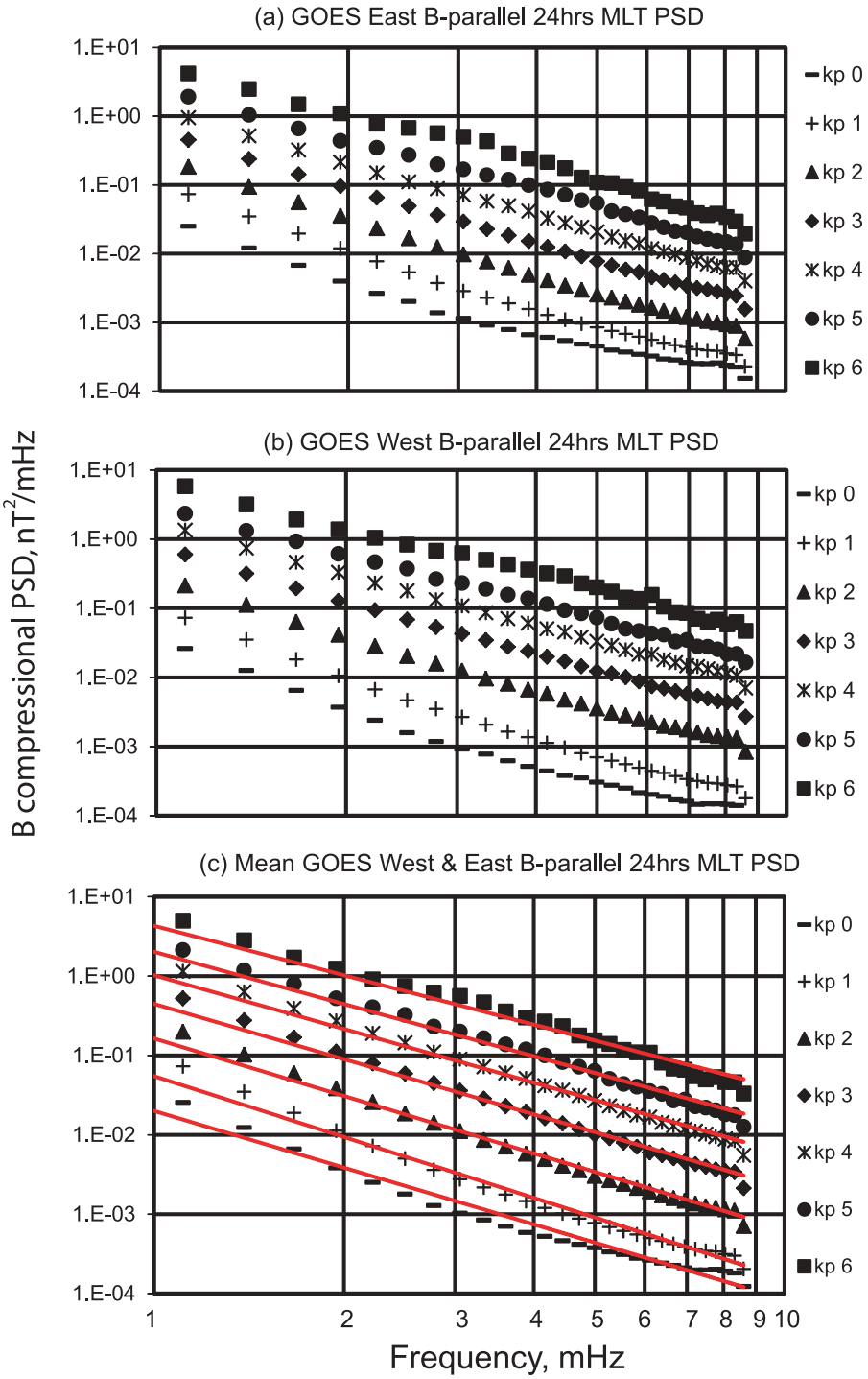

Figure 5. Median compressional magnetic field PSD averaged over 24 h MLT from 1996 to 2005 using (a) GOES East (b) GOES West and (c) the mean of the GOES East and West PSD values shown in Figures 5a and 5b. The results are binned with Kp and fitted to the power laws represented graphically by the solid lines and in functional form by the equations in Table 1.

where the satellites are outside the magnetopause, we have calculated the magnetopause stand-off distance by balancing the magnetic pressure inside the magnetosphere to the solar wind dynamic pressure using the solar wind parameters from the OMNI database and assuming a dipole magnetic field model for the Earth's field. Any day that the magnetopause stand-off distance is within 1 Re of geosynchronous altitude is omitted from our statistics. Consequently, for Kp > 6 there is a limited number of PSD statistics so that the median PSDs with Kp > 6 appear much more noisy compared to the median PSD values with Kp < 6. In our analysis we only use the median GOES PSD values determined for Kp-values ≤ 6 where there is a large enough number of events to accurately characterize the median PSD values.

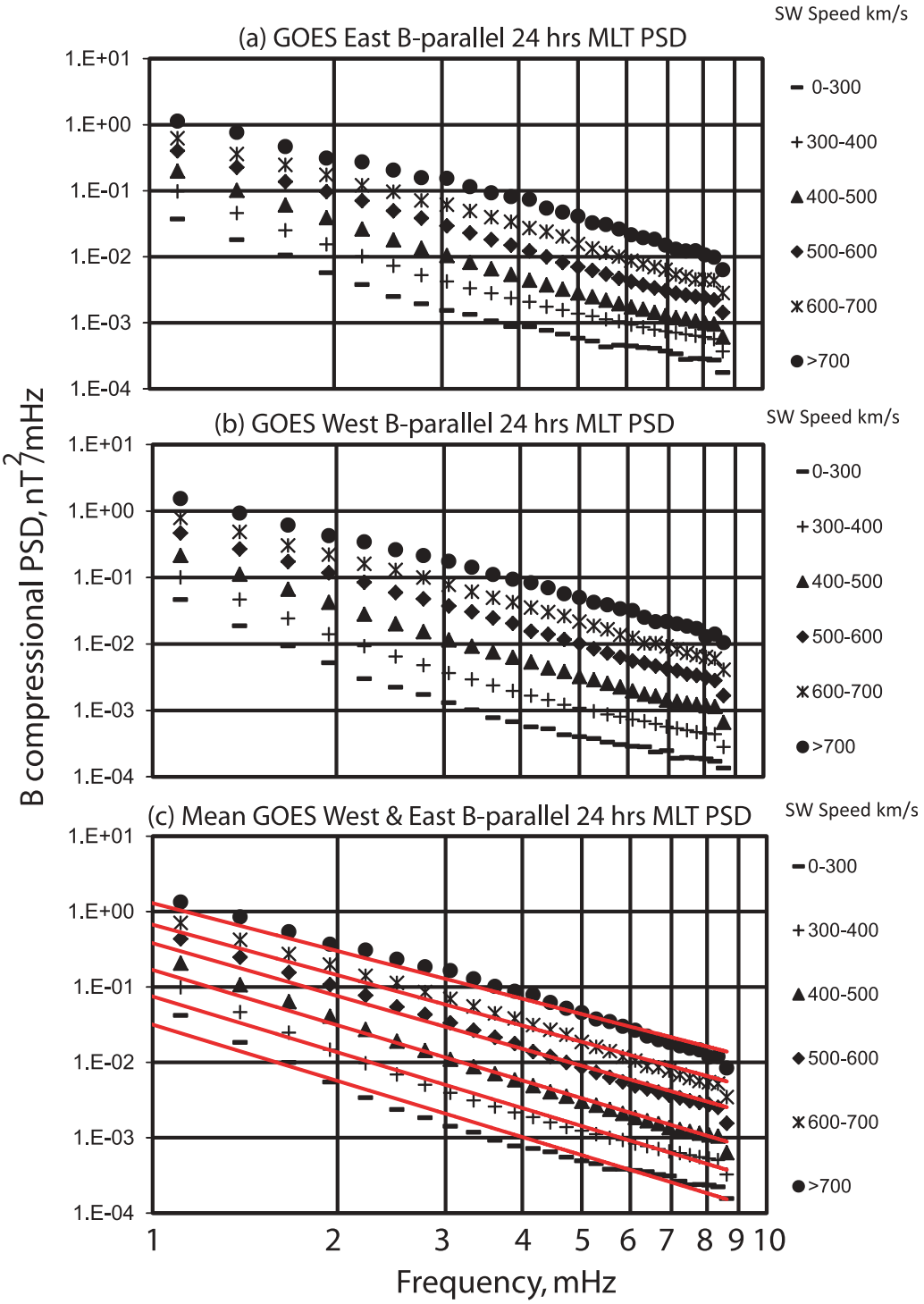

Figure 6. Median compressional magnetic field PSD measured over 24 h MLT from 1996 to 2005 using (a) GOES East (b) GOES West and (c) the mean of GOES East and West values shown in Figures 6a and 6b. The results are binned with solar wind speed and fitted to the power laws represented graphically by the solid lines and in functional form by the equations in Table 2.

[24] The GOES magnetic field PSD results can only be used to determine the magnetic diffusion coefficient at L = 6.6. However, in order for the diffusion coefficients to be used in equation (1) to simulate the flux variation of the outer radiation belt electrons, the diffusion coefficients must be known as a function of L-shell throughout the outer radiation belt region. To determine the L-shell variation of the magnetic field diffusion coefficients, we have also used the equatorial compressional magnetic field PSD results measured using AMPTE at L = 2.5–3.5, 3.5–4.5, 4.5–5.5 and 5.5–6.5 presented by *Takahashi and Anderson* [1992,

Table 1. GOES Compressional Magnetic Field Power Spectral Density (PSD) Fitted to a Power Law Function of Frequency for Different Kp Values[a]

	Kp Values						
Fits	0	1	2	3	4	5	6
A_{KP}	0.02	0.054	0.163	0.445	1.021	2.018	4.293
B_{KP}	2.37	2.54	2.40	2.31	2.24	2.18	2.06
R^2	0.914	0.935	0.940	0.942	0.943	0.946	0.935

[a] $PSD = A_{KP} f^{-BKP}$

Figure 5]. We approximate the equatorial compressional magnetic field PSD results presented by *Takahashi and Anderson* [1992, Figure 5] over the frequency range 1–15 mHz by the power laws shown in Table 3.

[25] The PSD results presented by *Takahashi and Anderson* [1992] were only shown for Kp = 2 intervals. In order to generate an estimate of the compressional magnetic field PSD for other Kp-values we assume that the same Kp dependence in the PSD amplitudes observed at L = 6.6 by GOES can also be extrapolated to the PSD amplitudes at lower L-shells measured by AMPTE, as expressed by the scale factors in Table 3. Our assumption that the same Kp dependence of PSD measured by GOES can be applied to the lower L-shell PSDs measured by AMPTE is consistent with the Kp dependence of the electric field PSD measured by CRRES [see *Brautigam et al.*, 2005, Figure 6]. *Brautigam et al.* [2005] showed that the electric field PSD values can be fitted to the function $P(L, Kp) = aL^b\exp(cKp)$ where the parameters a, b and c are frequency dependent [see *Brautigam et al.*, 2005, Table 3]. Our mapped electric field PSDs also show the same Kp dependence across L-shells from L = 6.5 down to L = 3.0 consistent with the CRRES electric field PSD measurements presented by *Brautigam et al.* [2005] as illustrated in our Figure 8. Figure 8a shows that the mapped electric field PSD has a similar decrease with L-shell across L-shells ranging from L = 3 to L = 6.5 for Kp = 2, 4 and 6. Similarly, Figure 8b shows that electric field PSD decreases with Kp with the same gradient at L-shells of L = 4.22, L = 5.40 and L = 6.51. Moreover, Figure 8b also shows that the electric field PSD decreases with solar wind speed again with the same gradient at L-shells of L = 4.22, L = 5.40 and L = 6.51. The solar wind speeds plotted at the top of Figure 8b correspond to the median solar wind speed averaged over each of the Kp bins.

[26] The GOES compressional PSD results are fitted to functions of both Kp and solar wind speed. However, the AMPTE compressional PSD results presented by *Takahashi and Anderson* [1992] are not binned with solar wind speed and are only presented for Kp = 2 intervals. For the magnetic diffusion coefficients to be derived as a function of the solar wind speed requires the dependence of the compressional magnetic field PSD on solar wind speed to be known both at GOES and at the lower L-shell measured by AMPTE to be known. In order to determine how the compressional magnetic field PSD measured by AMPTE scales with solar wind speed we have assumed that Kp = 2 corresponds to a solar wind interval of 400–500 km/s. This assumption is based on the PSD measurements made by GOES, which show that the median PSD measured during the Kp = 2 intervals and the solar wind speed bin of 400–500 km/s are approximately equal; see the GOES PSD fits in Table 1 and Table 2. In addition, similar to the Kp scaling of the AMPTE PSD we also assume that the same solar wind speed dependence observed by GOES at L = 6.6 can also be extrapolated to the PSD amplitudes at lower L-shells measured by AMPTE, as expressed by the scale factors in Table 4. This scaling is also consistent with our mapped electric field PSD values which show a similar scaling with solar wind speed at L-shells of L = 4.22, L = 5.40 and L = 6.51 as illustrated in Figure 8b.

Table 2. GOES Compressional Magnetic Field Power Spectral Density Fitted to a Power Law Function of Frequency for Different Solar Wind Speed Intervals[a]

	Solar Wind Speed (km/s)					
Fits	0–300	300–400	400–500	500–600	600–700	>700
A_{SW}	0.031	0.074	0.168	0.380	0.671	1.292
B_{SW}	2.47	2.45	2.43	2.32	2.22	2.10
R^2	0.920	0.932	0.940	0.935	0.933	0.932

[a] $PSD = A_{SW} f^{-BSW}$

3. Diffusion Coefficient Results

[27] The resulting combined compressional magnetic field PSD arising from the AMPTE and GOES measurements are

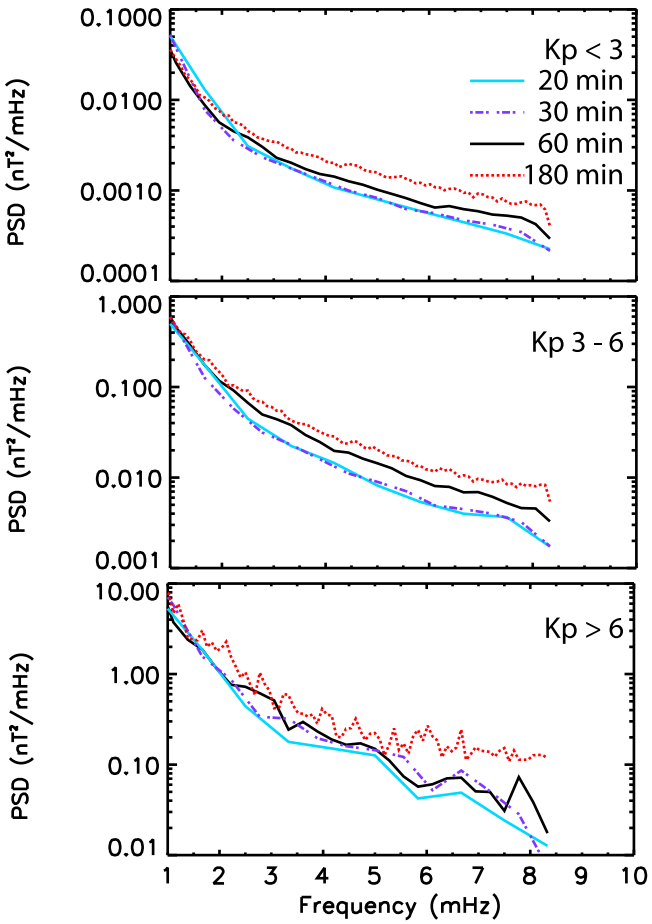

Figure 7. Comparison of the median GOES East compressional magnetic field PSDs obtained using window lengths of 20, 30, 60 and 180 min binned with Kp.

Table 3. Power Law Fits to the Compressional Magnetic Field PSD Results Presented by *Takahashi and Anderson* [1992, Figure 5] Over the Frequency f_B Range 1–15 mHz[a]

L-Shell Bin Range	Average L-Shell	Equatorial Magnetic Field b_z, PSD Power Law Fit (nT^2/Hz), Where $\boldsymbol{F_{KP} = A_{KP}(KP)/A_{KP}(KP = 2)}$ and $\boldsymbol{X_{KP} = B_{KP}(Kp)/B_{KP}(Kp = 2)}$
2.5–3.5	3.0	$F_{KP} \times 10^{1} \times f_B^{-1.3XKP}$
3.5–4.5	4.0	$F_{KP} \times 10^{1.2} \times f_B^{-1.9XKP}$
4.5–5.5	5.0	$F_{KP} \times 10^{1.3} \times f_B^{-1.9XKP}$
5.5–6.5	6.0	$F_{KP} \times 10^{1.5} \times f_B^{-1.9XKP}$

[a]The scale factors F and X produce the same Kp scaling observed at GOES, where the values of A_{KP} and B_{KP} are given in Table 1.

used in equation (3) to determine the magnetic field diffusion coefficient. Equation (3) illustrates that the magnetic field diffusion coefficient scales proportional to m^2. In order to examine if higher m-value waves are able to provide more rapid radial transport of electrons we have determined the magnetic field diffusion coefficients illustrated in Figure 9 assuming two values, $m = 1$ and $m = 10$. Figure 9 illustrates that increasing the m-value of the waves from $m = 1$ to $m = 10$ has negligible impact on the diffusion coefficient value, even though the value of the scale factor in equation (3) has increased by a factor of $m^2 = 100$. The reason increasing the wave m-value has not significantly affected the magnetic field diffusion coefficient is because increasing m also increases the resonant wave frequency and at higher wave frequencies the magnetic field PSD is much lower as illustrated in equation (6) and Figure 6. Similarly, Figure 9 shows that the value of the first adiabatic invariant, M, also does not significantly affect the value of magnetic field diffusion coefficient even though the diffusion coefficient scales $\propto M^2$ (see equation (3)). Again this is due to the fact that at higher M-values the resonant wave frequency is higher, and at these higher frequencies the value of the magnetic field PSD is lower; see Figure 5. The effects combine to create a very weak dependence on either M or m-value for the magnetic diffusion coefficient.

[28] In contrast, the electric field diffusion coefficient, D_{LL}^{E}, does not contain scale factors which depend on the wave azimuthal wave number, m, or the first adiabatic invariant, M (see equation (2)). In addition, the value of the wave's electric field PSD does not strongly decrease with frequency, like the magnetic field PSD (compare Figure 5 and Figure 4). Consequently, for higher M-values or m-values where the resonant wave frequency is higher, for the range of resonant frequencies considered here even the electric field diffusion coefficients are only changed slightly, as shown in Figure 10.

[29] To observationally determine the wave's m-value would require coherent measurements of the same wave by multiple longitudinally spaced instruments at the same time and latitude on the ground [see, e.g., *Chisham and Mann*, 1999]. In situ measurements of wave m-values in space are even more difficult to obtain, requiring multiple longitudinally spaced spacecraft measurements at the same radial and latitudinal position. Consequently, in order to derive the electric and magnetic field diffusion coefficients we have assumed that the wave's aziumthal wave number spectrum is constant consisting of a single azimuthal wave number at all frequencies, at all L-shells and for all Kp-values and solar wind speeds. In reality, the wave's m-value spectrum may depend on all these parameters. However, the results illustrated in Figure 9 and Figure 10 indicate that the diffusion coefficients do not strongly depend on the value of the resonant wave frequency or the m-value of the wave.

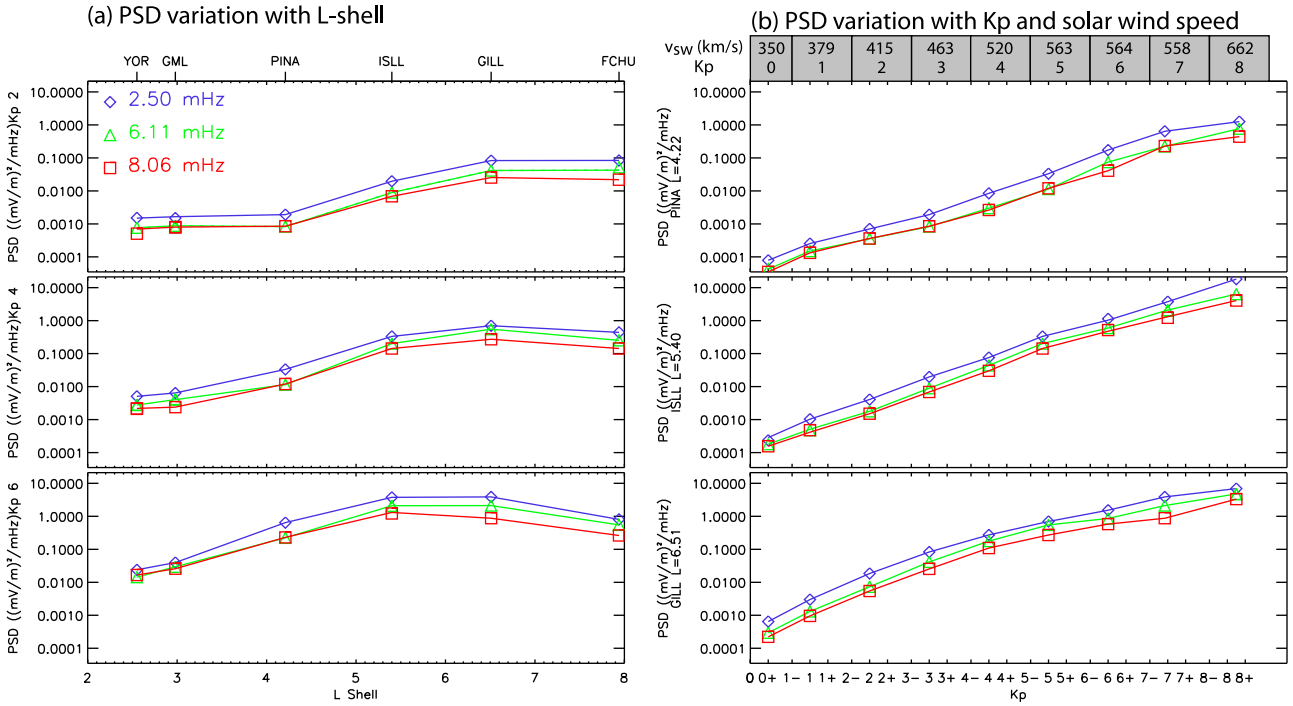

Figure 8. Mapped electric field PSD values at frequencies of 2.50, 6.11 and 8.06 mHz as (a) functions of L-shell for Kp values of 2, 4 and 6 and (b) functions of Kp and solar wind speed at L-shells of $L = 4.22$ (PINA), $L = 5.40$ (ISLL) and $L = 6.51$ (GILL).

Table 4. Power Law Fits to the Compressional Magnetic Field PSD Results Presented by *Takahashi and Anderson* [1992, Figure 5] Over the Frequency f_B Range 1–15 mHz[a]

L-Shell Bin Range	Average L-Shell	Equatorial Magnetic Field b_z, PSD Power Law Fit (nT^2/Hz), Where $F_{SW} = A_{SW}(SWB)/A_{SW}(SWB = 450)$ and $X_{SW} = B_{SW}(SWB)/B_{SW}(SWB = 450)$
2.5–3.5	3.0	$F_{SW} \times 10^{1} \times f_B^{-1.3XSW}$
3.5–4.5	4.0	$F_{SW} \times 10^{1.2} \times f_B^{-1.9XSW}$
4.5–5.5	5.0	$F_{SW} \times 10^{1.3} \times f_B^{-1.9XSW}$
5.5–6.5	6.0	$F_{SW} \times 10^{1.5} \times f_B^{-1.9XSW}$

[a]The scale factors F_{SW} and X_W produces the same solar wind speed scaling observed at GOES. The PSD results presented by *Takahashi and Anderson* [1992, Figure 5] for Kp = 2 are assumed to be equivalent to a solar wind speed bin of 400–500 km/s. The *SWB* values of 200, 350, 450, 550, 650 and 750 used in the fits below correspond to solar wind speed bins of 0–300, 300–400, 400–500, 500–600, and >700 km/s, respectively.

Consequently, the choice of *m*-value may not be critical for the derivation of the electric or magnetic field diffusion coefficients. In the rest of the paper we assume $m = 1$ unless specified otherwise.

[30] The diffusion coefficients required in equation (1) must be expressed as a function of L-shell for a fixed first adiabatic invariant *M*. Figure 10 illustrates the electric field diffusion coefficients determined at the discrete assumed dipole L-shell positions of the ground stations for M-values of 500 and 5000 MeV/G. The solid ($m = 1$) and dashed ($m = 10$) lines in Figure 10 show that the electric diffusion coefficients can be fitted to a power law which allows the diffusion coefficients at L-shells in-between the ground station positions to be easily determined. Similarly, Figure 9 shows that the variation with L-shell of the magnetic field diffusion coefficients also fits remarkably well to a power law, even though the diffusion coefficients at $L = 6.6$ are derived from PSD measurements made onboard GOES using data from 1996 to 2005 while the diffusion coefficients on the lower L-shells are derived from AMPTE measurements made during a different time interval (1984–1989).

[31] In what follows, we compare our diffusion coefficients D_{LL}^{E} [mapping] and D_{LL}^{B} [space] with those determined from the in situ CRRES electric field PSD measurements presented by *Brautigam et al.* [2005] (hereinafter referred as D_{LL}^{E} [CRRES]), the substorm convection electric field driven diffusion coefficient model presented by *Brautigam and Albert* [2000] (hereinafter referred to as D_{LL}^{E} [B & A]) and the previous magnetic field diffusion coefficients given by *Brautigam and Albert* [2000] (hereinafter referred to as D_{LL}^{B} [B & A]). The magnetic field diffusion coefficients D_{LL}^{B} [B & A] are based on ground magnetic field measurements at $L = 4$ mapped to equatorial plane compressional fields using the technique from *Lanzerotti and Morgan* [1973] and 1 month of in situ ATS 6 measurements at $L = 6.6$.

3.1. Comparison of the Electric Field Diffusion Coefficients

[32] The electric field diffusion coefficients determined using our mapping technique D_{LL}^{E} [mapping] are within an order of magnitude of those determined from the CRRES measurements D_{LL}^{E} [CRRES]. This agreement between the

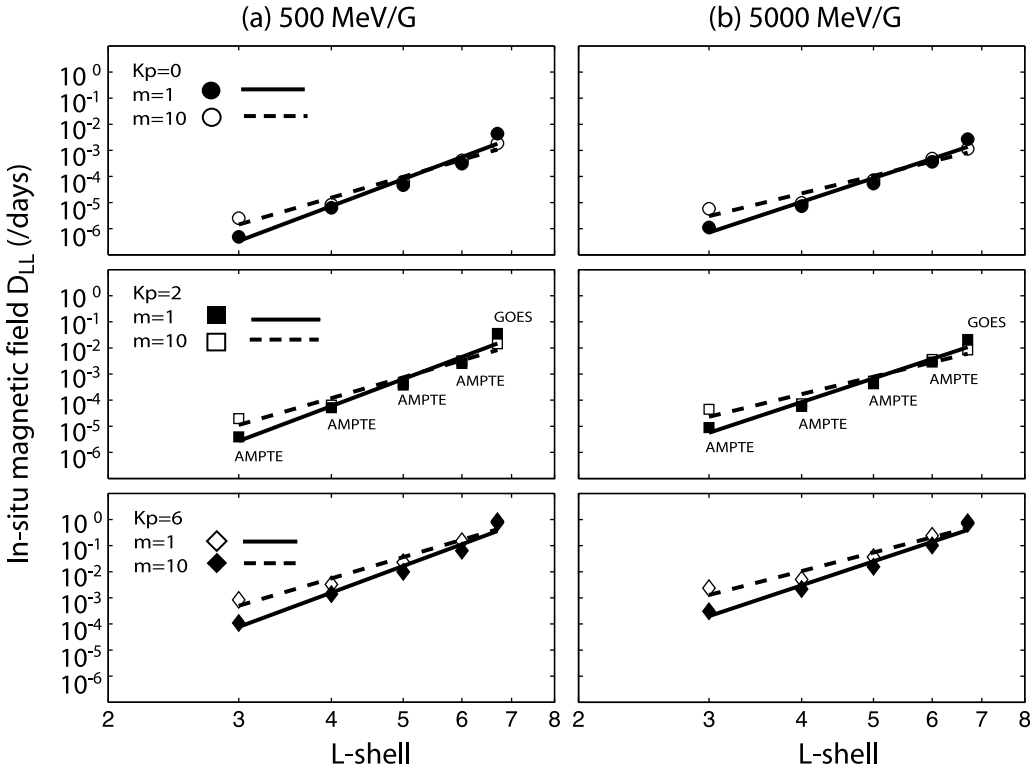

Figure 9. Magnetic field diffusion coefficients derived from in situ magnetic field PSDs measured by AMPTE at $L = 3$, 4, 5, and 6 as well as GOES at $L = 6.6$. The shaded and un-shaded symbols represent diffusion coefficients derived assuming $m = 1$ and $m = 10$, respectively. The solid and dashed lines represent power law fits to these diffusion coefficients for M-values of (a) 500 MeV/G and (b) 5000 MeV/G.

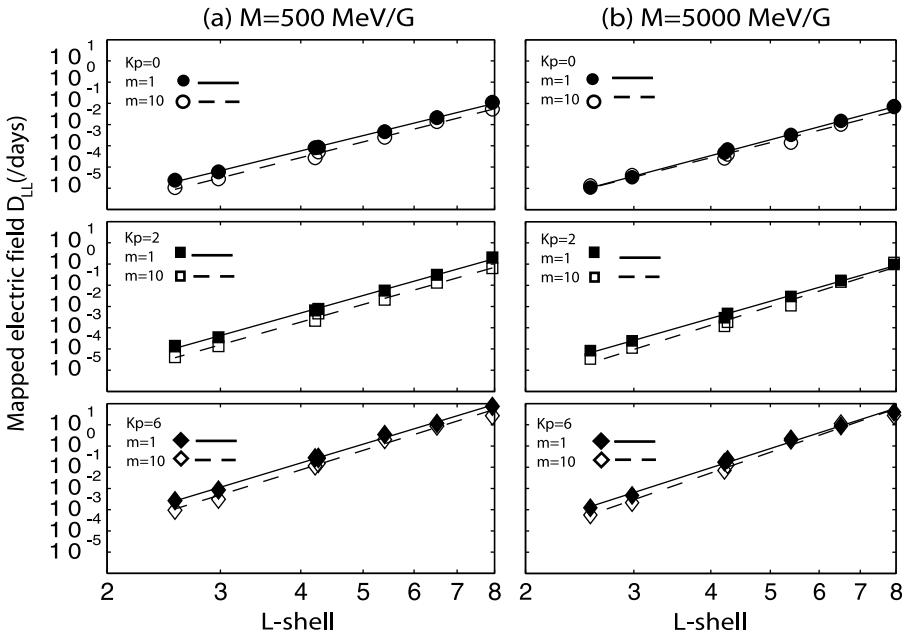

Figure 10. Electric field diffusion coefficients derived from ground magnetic field PSDs mapped to electric field PSDs in space in the equatorial plane with *m*-values of 1 and 10. The solid and dashed lines represent power law fits to these diffusion coefficients for M-values of (a) 500 MeV/G and (b) 5000 MeV/G.

diffusion coefficients is expected since our ground magnetometer mapped electric field PSDs are in excellent agreement with the PSD presented by *Brautigam et al.* [2005]. Both D_{LL}^{E} [CRRES] and D_{LL}^{E} [mapping] show a slight M-value dependence. However, the substorm convection electric field driven model D_{LL}^{E} [B & A] shows a strong decrease with energy dropping by over 2 orders of magnitude as M increases from 100 MeV/G to 5000 MeV/G; see Figure 11. The substorm driven electric field diffusion coefficients used by *Brautigam and Albert* [2000] are given by

$$D_{LL}^{E}[\text{B \& A}] = \frac{1}{4}\left[\frac{E_{rms}}{B_E}\right]^2\left[\frac{T}{1+(\omega_d T/2)^2}\right]L^6, \qquad \omega_d = \left[\frac{3M}{qL^2R_E^2}\right]\left[1+\frac{2MB_E}{m_e c^2 L^3}\right]^{-1/2} \tag{14}$$

Here T represents the exponential decay time of the substorm convection electric field (assumed to be 0.75 h). In the work by *Brautigam and Albert* [2000] the electric field E_{rms}, based on data from *Lyons and Schulz* [1989] and *Lyons and Thorne* [1973], is assumed to be given by

$$E_{rms}(Kp) = 0.26(Kp-1) + 0.1\,mV/m, Kp = 1\,to\,6. \tag{15}$$

The reason why the D_{LL}^{E} [B & A] lines in Figure 11 decrease with M-value can be understood from equation (14). As the M-value increases the electron drift speed increases, causing the value of D_{LL}^{E} [B & A] to be reduced.

3.2. Comparison of the Magnetic Field Diffusion Coefficients

[33] In the derivation of the magnetic field diffusion coefficients from the in situ measured magnetic field PSD we have assumed that all of the waves have a positive azimuthal wave number, m, so that they propagate in the same direction as the electrons and transfer the maximum amount of energy to the electrons through a symmetric drift resonance (see equation (6)). In reality, some of the waves will have negative m-values (especially for solar wind driven waves in the morning sector) and will not contribute to the diffusion coefficients, D_{LL}^{B} [space] (see equation (3)). Consequently, our diffusion coefficients D_{LL}^{B} [space] represent an upper limit to the magnetic field diffusion coefficients possible based on the in situ magnetic field PSD measured by AMPTE presented by *Takahashi and Anderson* [1992] and by GOES illustrated in Figure 5. However, the magnetic field diffusion coefficient D_{LL}^{B} [B & A] derived by mapping the magnetic field PSD from the ground to the magnetic field PSD in space using the *Lanzerotti and Morgan* [1973] expression and presented by *Brautigam and Albert* [2000] is much larger than our D_{LL}^{B} [space]; see Figure 11. Across all L shells, D_{LL}^{B} [B & A] is $\sim$100 times greater than D_{LL}^{B} [space]. Consequently, a radial diffusion model of the radiation belts based on the D_{LL}^{B} [B & A] coefficients would result in electron transport at least 100 times faster than models based on in situ measurements of the magnetic field PSD such as those presented here. The magnetic field diffusion coefficient D_{LL}^{B} [B & A] derived by *Brautigam and Albert* [2000] is expressed analytically as

$$D_{LL}^{B}[\text{B \& A}] = 10^{(0.506Kp-9.325)}L^{10}, \; Kp = 1\,to\,6. \tag{16}$$

Equation (16) shows that D_{LL}^{B} [B & A] as expressed does not depend on the M-value of the electrons, as is also illustrated in Figure 11. The magnetic field diffusion coefficients derived from the AMPTE and GOES measurements of the PSD, D_{LL}^{B} [space], however, show a slight decrease with increasing M-value; see Figure 11.

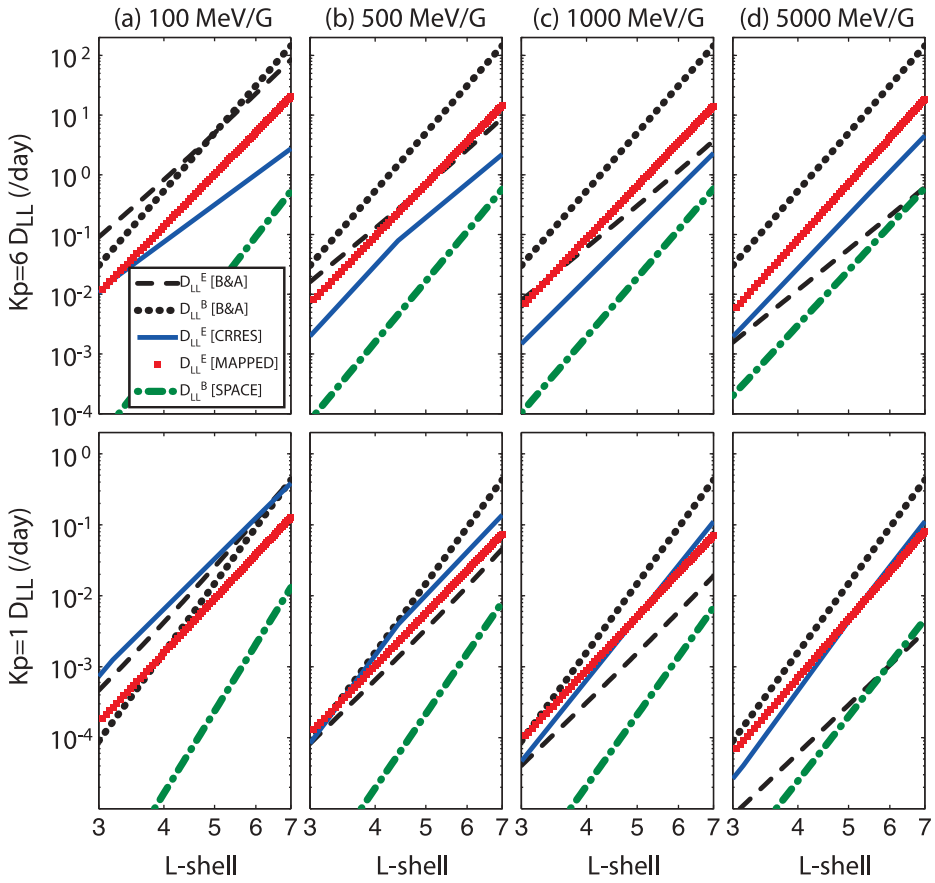

Figure 11. A comparison of the electric field and magnetic field diffusion coefficients derived in this paper with theoretically derived electric field diffusion coefficient from *Brautigam and Albert* [2000] D_{LL}^{E} [B & A], the magnetic diffusion coefficient from *Brautigam and Albert* [2000] D_{LL}^{B} [B & A], and the electric field diffusion coefficient obtain from CRRES PSD measurements presented by *Brautigam et al.* [2005] D_{LL}^{E} [CRRES]. For Kp-values of 1 and 6 with first adiabatic invariant M-values of (a) 100 MeV/G (b) 500 MeV/G, (c) 1000 MeV/G and (d) 5000 MeV/G.

3.3. Comparison of the Electric Field and Magnetic Field Diffusion Coefficients

[34] Based on the electric and magnetic field diffusion coefficients derived by *Brautigam and Albert* [2000], it is clear that D_{LL}^{B} [B & A] dominates over the electric field diffusion coefficient D_{LL}^{E} [B & A]. Moreover, radial diffusion simulations using the *Brautigam and Albert* [2000] formulation for radial diffusion coefficients, such as the simulations presented by *Shprits et al.* [2005], only include D_{LL}^{B} [B & A] justifying neglecting the electric field diffusion on the basis that D_{LL}^{B} [B & A] $>>$ D_{LL}^{E} [B & A]. However, in contrast to this assumption, our results indicate that the electric field diffusion coefficients D_{LL}^{E} [mapping] dominate over the magnetic field diffusion coefficients D_{LL}^{B} [space] for all L-shells and Kp values; see Figure 11.

4. Discussion and Conclusions

[35] Understanding how the electric and magnetic field PSD of ULF waves varies with time in the equatorial plane is critically important for the development of ULF wave radial diffusion simulations of the radiation belts. Collecting a large database of ULF wave PSD values during intervals with different Kp-values or solar wind speeds allows the PSD to be predicted as a function of Kp or solar wind speed and hence as a function of time. In situ spacecraft measurements of ULF wave electric and magnetic fields can provide good estimates of the PSD. However, typically in situ measurements of the PSD have only been taken over short time intervals such as the CRRES electric field PSD results presented by *Brautigam et al.* [2005], or from a limited L-shell range such as the GOES magnetic field PSD results presented by *Huang et al.* [2010]. The in situ CRRES PSD measurements were taken during a 10 month period, and using this database, *Brautigam et al.* [2005] characterized the electric field PSD as a function of Kp for values ranging from Kp = 1 to Kp = 6; for Kp = 0 and Kp > 6 the CRRES statistical database of PSD events was too low to characterize the PSD.

[36] Here we used over 15 years of ground magnetic field PSD measurements, which are mapped to the equatorial electric field PSD, to characterize the electric field PSD as a function of Kp with values ranging from Kp = 0 to Kp = 9 and also as function of solar wind speed. Our estimates of the azimuthal electric field PSD as a function of Kp are in good agreement with the in situ CRRES electric field PSD results presented by *Brautigam et al.* [2005], both data sets illustrating clear peaks in PSD at ~4 mHz on L-shells between 4 and 6. The characterization of the electric field PSD as a

function of solar wind speed also allows a near real-time specification of the electric field diffusion coefficients using available near real time solar wind data from L1.

[37] To determine the magnetic field PSD, we used GOES East and West measurements taken from 1996 to 2005 to characterize the compressional magnetic field PSD as a function of Kp, for values ranging from Kp = 0 to Kp = 6, and also as a function of solar wind speed. Our GOES magnetic field PSD estimates are in excellent agreement with the GOES magnetic field PSD results given by *Huang et al.* [2010]. Due to the geostationary orbit of the GOES spacecraft, these measurements are only possible at L = 6.6. However, to determine the magnetic field PSD at different L-shells, the GOES PSD results are supplemented with AMPTE measurements of the compressional magnetic field PSD at L = 3, L = 4 and L = 5 for Kp = 2 as presented by *Takahashi and Anderson* [1992]. By merging these GOES and AMPTE data sets we characterized the compressional magnetic field PSD with L-shell and Kp or solar wind speed.

[38] At L = 6.6 our magnetic field diffusion coefficients derived from the 9 year statistical database of GOES East and West measurements are approximately 2 orders of magnitude lower than that given by the magnetic field diffusion coefficient model presented by *Brautigam and Albert* [2000], D_{LL}^{B} [B & A]. However, in the work by *Brautigam and Albert* [2000] the magnetic field diffusion coefficients are not based on in situ measurements of the compressional magnetic field PSD in the equatorial plane. Instead the diffusion coefficients are derived from PSD measurements made using 1 month of in situ ATS 6 measurements at L = 6.6 and ground magnetometer measurements at L = 4 mapped to the equatorial plane in space using a mapping model based on symmetric oscillations of a dipole magnetic field with no wave propagation or ionospheric effects included [see *Lanzerotti and Morgan*, 1973].

[39] Our results present a new ULF wave based formalism for representing both electric and magnetic radial diffusion coefficients in the magnetosphere. Our parameterizations of the ULF power as a function of frequency, L-shell, and Kp or solar wind speed represent an alternative to the traditional more empirical basis of the diffusion coefficients presented, for example, by *Brautigam and Albert* [2000]. Moreover, we present best fits to the ULF wave PSD data, which allows diffusion coefficients to be easily derived.

[40] Significantly, our results indicate that both the electric and magnetic field diffusion coefficients should be included in radial diffusion simulations of the radiation belts, in contrast to previous assertions that the electric field component can be neglected. Moreover, it is the electric field diffusion coefficient which dominates over the magnetic field diffusion coefficients across all L-shells spanning the outer radiation belt, as illustrated in Figure 11.

[41] **Acknowledgments.** I. R. Mann is supported by a Discovery Grant from Canadian NSERC. This work is supported by the Canadian Space Agency. A. A. Chan is supported by NASA grants NNX08AM36G and NNX10AL02G. We acknowledge the WDC for Geomagnetism, Kyoto University, Japan, for the geomagnetic indices and CDAWeb for GOES and solar wind speed data. The CANOPUS magnetometer array (now CARISMA; http://www.carisma.ca) is operated by the University of Alberta and funded by the Canadian Space Agency. The Sub-Auroral Magnetometer Network (SAMNET) is operated by the Space Plasma Environment and Radio Science (SPEARS) group, Department of Physics, Lancaster University.

[42] Robert Lysak thanks the reviewers for their assistance in evaluating this paper.

References

Brautigam, D. H., and J. M. Albert (2000), Radial diffusion analysis of outer radiation belt electrons during the October 9, 1990, magnetic storm, *J. Geophys. Res.*, *105*(A1), 291–309, doi:10.1029/1999JA900344.

Brautigam, D. H., G. P. Ginet, J. M. Albert, J. R. Wygant, D. E. Rowland, A. Ling, and J. Bass (2005), CRRES electric field power spectra and radial diffusion coefficients, *J. Geophys. Res.*, *110*, A02214, doi:10.1029/2004JA010612.

Brizard, A. J., and A. A. Chan (2001), Relativistic bounce-averaged quasilinear diffusion equation for low-frequency electromagnetic fluctuations, *Phys. Plasmas*, *8*(11), 4762–4771, doi:10.1063/1.1408623.

Chisham, G., and I. R. Mann (1999), A Pc5 ULF wave with large azimuthal wavenumber observed within the morning sector plasmasphere by Sub-Auroral Magnetometer Network, *J. Geophys. Res.*, *104*(A7), 14,717–14,727, doi:10.1029/1999JA900147.

Clemmons, J. H., et al. (2000), Observations of traveling Pc5 waves and their relation to the magnetic cloud event of January 1997, *J. Geophys. Res.*, *105*(A3), 5441–5452, doi:10.1029/1999JA900418.

Cornwall, J. M. (1968), Diffusion processes influenced by conjugate-point wave phenomena, *Radio Sci.*, *3*(7), 740–744.

Cross, R. C. (1988a), Torsional Alfvén modes in dipole and toroidal magnetospheres, *Planet. Space Sci.*, *36*(12), 1461–1468, doi:10.1016/0032-0633(88)90011-6.

Cross, R. C. (1988b), *An Introduction to Alfven Waves*, 1st ed., Taylor and Francis, Bristol, U. K.

Fälthammar, C.-G. (1965), Effects of time-dependent electric fields on geomagnetically trapped radiation, *J. Geophys. Res.*, *70*(11), 2503–2516, doi:10.1029/JZ070i011p02503.

Fei, Y., A. A. Chan, S. R. Elkington, and M. J. Wiltberger (2006), Radial diffusion and MHD particle simulations of relativistic electron transport by ULF waves in the September 1998 storm, *J. Geophys. Res.*, *111*, A12209, doi:10.1029/2005JA011211.

Glassmeier, K.-H. (1984), On the influence of ionospheres with non-uniform conductivity distribution on hydromagnetic waves, *J. Geophys.*, *54*(3), 125–137.

Holzworth, R. H., and F. S. Mozer (1979), Direct evaluation of the radial diffusion coefficient near L = 6 due to electric field fluctuations, *J. Geophys. Res.*, *84*(A6), 2559–2566, doi:10.1029/JA084iA06p02559.

Huang, C.-L., H. E. Spence, M. K. Hudson, and S. R. Elkington (2010), Modeling radiation belt radial diffusion in ULF wave fields: 2. Estimating rates of radial diffusion using combined MHD and particle codes, *J. Geophys. Res.*, *115*, A06216, doi:10.1029/2009JA014918.

Hughes, W. J., and D. J. Southwood (1976), The screening of micropulsation signals by atmosphere and ionosphere, *J. Geophys. Res.*, *81*(19), 3234–3240, doi:10.1029/JA081i019p03234.

Kivelson, M. G., and D. J. Southwood (1988), Hydromagnetic waves and the ionosphere, *Geophys. Res. Lett.*, *15*(11), 1271–1274, doi:10.1029/GL015i011p01271.

Lanzerotti, L. J., and C. G. Morgan (1973), ULF geomagnetic power near L = 4: 2. Temporal variation of radial diffusion coefficient for relativistic electrons, *J. Geophys. Res.*, *78*(22), 4600–4610, doi:10.1029/JA078i022p04600.

Lyons, L. R., and M. Schulz (1989), Access of energetic particles to storm time ring current through enhanced radial "diffusion," *J. Geophys. Res.*, *94*(A5), 5491–5496, doi:10.1029/JA094iA05p05491.

Lyons, L. R., and R. M. Thorne (1973), Equilibrium structure of radiation belt electrons, *J. Geophys. Res.*, *78*(13), 2142–2149, doi:10.1029/JA078i013p02142.

Mann, I. R., A. N. Wright, and A. W. Hood (1997), Multiple-timescales analysis of ideal poloidal Alfvén waves, *J. Geophys. Res.*, *102*(A2), 2381–2390, doi:10.1029/96JA03034.

Mann, I. R., et al. (2008), The upgraded CARISMA magnetometer array in the THEMIS era, *Space Sci. Rev.*, *141*(1–4), 413–451, doi:10.1007/s11214-008-9457-6.

Ozeke, L. G., I. R. Mann, and J. T. Mathews (2005), The influence of asymmetric ionospheric Pedersen conductances on the field-aligned phase variation of guided toroidal and guided poloidal Alfvén waves, *J. Geophys. Res.*, *110*, A08210, doi:10.1029/2005JA011167.

Ozeke, L. G., I. R. Mann, and I. J. Rae (2009), Mapping guided Alfvén wave magnetic field amplitudes observed on the ground to equatorial electric field amplitudes in space, *J. Geophys. Res.*, *114*, A01214, doi:10.1029/2008JA013041.

Rae, I. J., et al. (2005), Evolution and characteristics of global Pc5 ULF waves during a high solar wind speed interval, *J. Geophys. Res.*, *110*, A12211, doi:10.1029/2005JA011007.

Rae, I. J., I. R. Mann, K. R. Murphy, L. G. Ozeke, D. K. Milling, A. A. A. Chan, S. R. Elkington, and F. Honary (2012), Ground-based magnetometer determination of in situ Pc4–5 ULF electric field wave spectra as a function of solar wind speed, *J. Geophys. Res.*, *117*, A04221, doi:10.1029/2011JA017335.

Schulz, M., and L. J. Lanzerotti (1974), *Particle Diffusion in the Radiation Belts*, *Phys. Chem. Space Ser.*, vol. 7, 215 pp., Springer, New York.

Shprits, Y. Y., R. M. Thorne, G. D. Reeves, and R. Friedel (2005), Radial diffusion modeling with empirical lifetimes: Comparison with CRRES observations, *Ann. Geophys.*, *23*(4), 1467–1471, doi:10.5194/angeo-23-1467-2005.

Southwood, D. J., and M. G. Kivelson (1982), Charged particle behavior in low-frequency geomagnetic pulsations: 2. Graphical approach, *J. Geophys. Res.*, *87*(A3), 1707–1710, doi:10.1029/JA087iA03p01707.

Takahashi, K., and B. J. Anderson (1992), Distribution of ULF energy ($f <$ 80 mHz) in the inner magnetosphere: A statistical analysis of AMPTE CCE magnetic field data, *J. Geophys. Res.*, *97*(A7), 10,751–10,773, doi:10.1029/92JA00328.

Van Allen, J. A., G. H. Ludwig, E. C. Ray, and C. E. McIlwain (1958), Observation of high intensity radiation by satellites 1958 Alpha and Gamma, *Jet Propul.*, *28*, 588–592.

Yeoman, T. K., D. K. Milling, and D. Orr (1990), Pi2 pulsation polarization patterns on the U.K. sub-auroral magnetometer network (SAMNET), *Planet. Space Sci.*, *38*(5), 589–602, doi:10.1016/0032-0633(90)90065-X.

A. A. Chan, Department of Physics and Astronomy, Rice University, PO Box 1892, Houston, TX 77251, USA.

S. R. Elkington, Laboratory for Atmospheric and Space Physics, University of Colorado at Boulder, 1234 Innovation Dr., Boulder, CO 80303, USA.

I. R. Mann, D. K. Milling, K. R. Murphy, L. G. Ozeke, and I. J. Rae, Department of Physics, University of Alberta, Edmonton, AB T6G 2E1, Canada. (lozeke@ualberta.ca)

H. J. Singer, Space Weather Prediction Center, NOAA, 325 Broadway, Boulder, CO 80305, USA.